Supporting Information

Highly fast and selective removal of nitrate in groundwater by bimetallic catalysts supported by fly ash-derived zeolite Na-X

Jaehyeong Park[a,b], Jong Kwon Choe[b], Woojin Lee[c], and Sungjun Bae[a*]

[a]Department of Civil and Environmental Engineering, Konkuk University, 120 Neungdong-ro, Gwangjin-gu, Seoul 05029, Republic of Korea

[b]Department of Civil and Environmental Engineering and Institute of Construction and Environmental Engineering, Seoul National University, 1 Gwanak-ro Gwanak-gu Seoul 08826

[c]Department of Civil and Environmental Engineering, Nazarbayev University, Astana 010000, Kazakhstan

*Corresponding author: bsj1003@konkuk.ac.kr

phone: +82-02-450-3904

A supporting information for *Environmental Science: Nano*

Supporting Information

Experimental: Materials and Chemicals

For the pretreatment of NMFA, deionized water (DIW, 18.3 MΩ cm, Human Power I+, Human corporation, Korea) and acetic acid (99.7 %, Dae Jung Chemical, Korea) were used. NaOH (bead, 97.0 %, Dae Jung Chemical, Korea) was used for the alkaline fusion of acetic acid-treated NMFA. Precursor solutions for Sn, Cu, Ni, Zn, Ag, Au, Pt, and Pd were prepared with tin(IV) chloride pentahydrate (98%, Sigma-Aldrich Inc., USA), copper(II) chloride dihydrate (≥99.0%, Sigma-Aldrich Inc., USA), nickel(II) chloride hexahydrate (97.0%, Samchun Pure Chemicals Co., Korea), zinc chloride (99.999%, Sigma-Aldrich Inc., USA), silver nitrate (≥99.0%, Sigma-Aldrich Inc., USA), gold(III) chloride trihydrate (≥99.9%, Sigma-Aldrich Inc., USA), platinum(IV) chloride (96%, Sigma-Aldrich Inc., USA), and Palladium(II) chloride (99%, Sigma-Aldrich Inc., USA), respectively. The other Pd-Sn bimetallic catalysts were fabricated using different support materials, i.e., silicon dioxide (~99%, 0.5-10 μm, Sigma-Aldrich, USA), aluminum oxide (99.5%, ≤10 μm, Sigma-Aldrich, USA) and molecular sieves 13X (C-13X, ~2 μm, Sigma-Aldrich Inc., USA). Sodium borohydride (98%, Sigma-Aldrich, USA) was used to activate bimetallic catalysts. Potassium nitrate (99.0%, Duksan Pure Chemical Co., Korea), Potassium nitrite (99.0%, Sigma-Aldrich Inc., USA) and ammonium chloride (98.5%, Shinyo Pure Chemicals Co., Japan) were used for stock and standard solutions for ion chromatography (IC). Sodium bicarbonate (99.0%, Samchun Pure Chemicals Co., Korea), sodium carbonate (99.95%, Sigma-Aldrich Inc., USA), sulfuric acid (60%, Dae Jung Chemical, Korea), and methanesurfonic acid (≥99.0%, Sigma-Aldrich Inc., USA) were used to prepare eluent for IC operation for the determination of anions and cations.

Experimental: Preparation of NMFA and Zeolite-XF

Supporting Information

We followed our previous method for the separation and pretreatment of NMFA.[1,2] Briefly, iron-rich fly ash particles were separated from CFA-DIW suspension using a neodymium magnet to obtain NMFA.[2] After washing with DIW and drying, 5.0 g of NMFA was further treated with a diluted solution of acetic acid (5 M) and then washed with DIW three times. Lastly, the resulting material was dried in an oven at 105 °C for 24 h.

For the synthesis of Zeolite-XF, we used a modified fusion method as illustrated in Scheme S1.[1,3] The acetic acid-treated NMFA (5.0 g) was mixed with 6.0 g of NaOH beads with a mass ratio 1:1.2 and ground into fine particles. This homogeneous mixture was transferred to a nickel crucible and calcined at 550 °C for 1 h in a muffle furnace (MF-10, Jeio-Tech, Korea) to convert Si–Al-containing minerals in the NMFA into sodium silicate and sodium aluminate. Then, the fused solids were ground, and 9.7 g of the sample was transferred into a polytetrafluoroethylene (PTFE) bottle containing 53.35 mL of DIW. The mixture was sonicated for 5 min and then continuously stirred (700 rpm) at 25 ± 0.5 °C for 24 h. After 24 h, the PTFE bottle was sealed and heated at 90 °C for 9 h for the crystallization of zeolite X. Lastly, the resulting zeolite was vacuum filtered, washed three times with DIW by centrifugation (7,000 rpm, 3 min), and oven-dried at 105 °C for 24 h. The zeolite obtained by our method was labeled Zeolite-XF, which indicates the phase of the zeolite (i.e., Na-X) identified by XRD analysis.

Experimental: Synthesis of Pd–Sn/Zeolite-XF

Bimetallic Pd–Sn/Zeolite-XF catalysts were prepared using a modified impregnation method [4]. Zeolite-XF (1.0 g) was added into a polypropylene bottle containing 90 mL of DIW, and the suspension was then sonicated for 5 min and continuously stirred at 700 rpm with a PTFE impeller. Sn and Pd precursor solutions were freshly prepared, and the given amounts of two precursors were sequentially added into the suspension with constant mechanical stirring (700 rpm) at room temperature (25 ± 0.2 °C) for 2 h. This mixture was oven-dried at 105 °C for 24 h. Then, the dried samples were calcined at 350 °C in a muffle furnace for 2 h to stabilize Pd and Sn on the zeolite-XF surface. Prior to nitrate reduction, an exact amount of Pd–Sn/Zeolite-XF (0.25 g) was mixed with 20.0 mL of DIW, the mixture was sonicated for 2 min, and an aqueous solution of 10 mM $NaBH_4$ was added dropwise. $NaBH_4$ was used to reduce Pd and Sn on the surface of Zeolite-XF. The activated Pd–Sn/Zeolite-XF was washed with DDIW twice in the anaerobic chamber to remove residual chemicals and used for batch experiments immediately. Other monometallic and bimetallic catalysts with different support materials were prepared similarly.

Experimental: Characterization of Zeolite-XF and catalysts

The powder XRD patterns of the raw CFA and Zeolite-XF were measured using Cu Kα radiation (Bruker DE/D8 Advance, Germany). The scan range was between 10° and 90° 2θ with a scan speed of $2^{\circ}\ \mathrm{min}^{-1}$. The BET specific surface area, pore volume, and pore size of Zeolite-XF were measured by nitrogen adsorption and desorption at −196 °C with a BET surface analyzer (3Flex, Micromeritics, USA).

For sample preparation of HR-FESEM/EDX (SU8010, Hitachi High-Technologies Corporation), FE-TEM/EDX (JEM-F200(TFEG), JEOL Ltd., Japan), and XPS (K-alpha, Thermo VG Scientific, USA), Pd–Sn/Zeolite-XF, after activation with $NaBH_4$, was transferred to the anaerobic chamber (Coylab) and rinsed with DDIW, 50% deaerated ethanol, and 100% deaerated ethanol sequentially. The sample for Pd–Sn/Zeolite-XF after NO_3^- reduction (reaction time = 90 min) was prepared as follows. After the reaction was complete, mechanical stirring and H_2 and CO_2 supply were turned off and Ar purging was started to avoid oxidation of the catalyst by O_2 in air. Then, the catalyst was collected through vacuum filtering using a mixed cellulose ester membrane filter (0.2 μm, Advantech, Japan) in the anaerobic chamber to minimize the surface oxidation by O_2 in air. The collected catalyst was washed with DDIW, 50% deaerated ethanol, and 100% deaerated ethanol sequentially. All washed samples were dispersed in deaerated ethanol to avoid further oxidation before the analyses.

The morphological characteristics of NMFA, Zeolite-XF, and Pd-Sn/Zeolite-XF after reaction were investigated using HR-FESEM (SU8010, Hitachi High Technologies Corporations) equipped with EDX. EDX mapping was conducted to identify the dispersion of Pd, Sn, Si, Al, O, and Na of Zeolite-XF, and Pd-Sn/Zeolite-XF. Pd-Sn/Zeolite-XF samples after activation and reaction were transferred to carbon tape on SEM template after completely drying deaerated ethanol, coated with Pt, and analyzed at 15.0 kV.

The morphology, d-spacing and the fast Fourier transformation (FFT) of Zeolite-XF, and the dispersion of Pd and Sn on the surface of Zeolite-XF after activation and reaction were analyzed by FE-TEM (JEM-F200(TFEG), JEOL Ltd, Japan) equipped with EDX (JEOL Dual SDD Type) at an acceleration voltage of 200 kV. Zeolite-XF and Pd-Sn/Zeolite-XF samples dispersed in deaerated ethanol were diluted and sonicated for 15 min, then droplets of the sample were carefully placed on Cu TEM grids in the anaerobic chamber.

The oxidation states of Pd and Sn on the surface of 1.5 wt.% Pd-0.5 wt.% Sn/Zeolite-XF before activation, after activation with $NaBH_4$, and after nitrate reaction were investigated by XPS (K-alpha, Thermo VG Scientific, USA) with Al Kα X-ray (1486.7 eV) radiation at a source power of 75 W. The C 1s peak at 285 eV was used as a reference for adjusting the surface charging effects. The narrow-scan spectra in the ranges 504-480 eV and 350–330 eV were obtained to identify the oxidation states of Sn and Pd species on the Pd-Sn/Zeolite-XF surface, respectively.

The zeta potentials of Zeolite-XF and Pd-Sn/Zeolite-XF at pH 3, 5, 7, and 9 were determined by a zeta potential analyzer (ELS-1000ZS, Otsuka Electronics). The catalyst was activated by $NaBH_4$ and added into the prepared solutions.

Supporting Information

Zeolite-XF, 1.5 wt.% Pd/Zeolite-XF, 0.5 wt.% Sn/Zeolite-XF, and 1.5 wt.% Pd-0.5 wt.% Sn/Zeolite-XF without activation with $NaBH_4$ were introduced into a conventional flow system for the TPR analysis (AutoChemII2920, Micromeritics Instrument Corp., USA) and examined in the temperature range of 50–1000 °C with ramping of 20°C /min. 10% H_2/Ar was passed through the system bed at flow rate of 10 cc/min.

H_2 pulse chemisorption was performed to determine the dispersion of metals on Zeolite-XF surface by AutoChemII2920 (Micromeritics Instrument Corp., USA). 1.5 wt.% Pd/Zeolite-XF and 1.5 wt.% Pd-0.5 wt.% Sn/Zeolite-XF before $NaBH_4$-induced activation were outgassed under vacuum, then reduced under the flow of 10% H_2/Ar for 2 h at 350 °C, followed by flushing with Ar for 1 h and cooling to 30 ºC. The chemisorption test was performed at 30 °C by pulsing the 10% H_2/Ar.

After the reaction for 90 min, 1 mL of the reaction mixture was sampled and filtered with 0.2 μm PVDF syringe filter and then diluted with 1% HNO_3 for the analysis. The diluted samples were analyzed with inductively coupled plasma-mass spectrometry (ICP-MS, 7800, Agilent, USA) to investigate the leaching of Pd, Sn, Cr, Mn, As, and Pb from the catalyst during NO_3^- and NO_2^- reduction.

Experimental: Procedures for parametric studies

The effect of promoter metals (Ag, Zn, Sn, Cu, and Ni) and noble metals (Pd, Pt, and Au) was investigated. The effects of Sn loading, Pd loading, and flow rates of H_2 and CO_2 on NO_3^- removal and selectivity of byproducts were investigated by using six different loadings of Sn (0, 0.5, 1.0, 1.5, 2.0, and 2.5 wt.%), six different loadings of Pd (0, 0.5, 1.0, 1.5, 2.0, and 2.5 wt.%), five different flow rates of H_2 (0, 15, 30, 45, and 60 mL/min) and four different flow rates of CO_2 (0, 20, 40, and 60 mL/min), respectively.

Supporting Information

The recycling test of 1.5 wt.% Pd-0.5 wt.% Sn/Zeolite-XF were performed at optimized conditions (i.e., 45 cc/min of H_2 and 40 cc/min of CO_2) to evaluate the reusability of the catalyst. After each cycle, the reaction mixture was purged with Ar gas after stopping H_2 and CO_2 supply to avoid oxidation of the used catalyst by atmospheric O_2. The reactor was transferred into anaerobic chamber immediately, and then the used catalyst was separated by vacuum filtration using a mixed cellulose ester membrane filter. The filtered catalyst was washed with DDIW. Subsequently, the suspension was added into the reactor containing 179.6 mL of DDIW, followed by purging with H_2 and CO_2 gas. The next cycle of reaction was initiated by injecting 0.4 mL of NO_3^- stock solution as illustrated above

.

Supporting Information

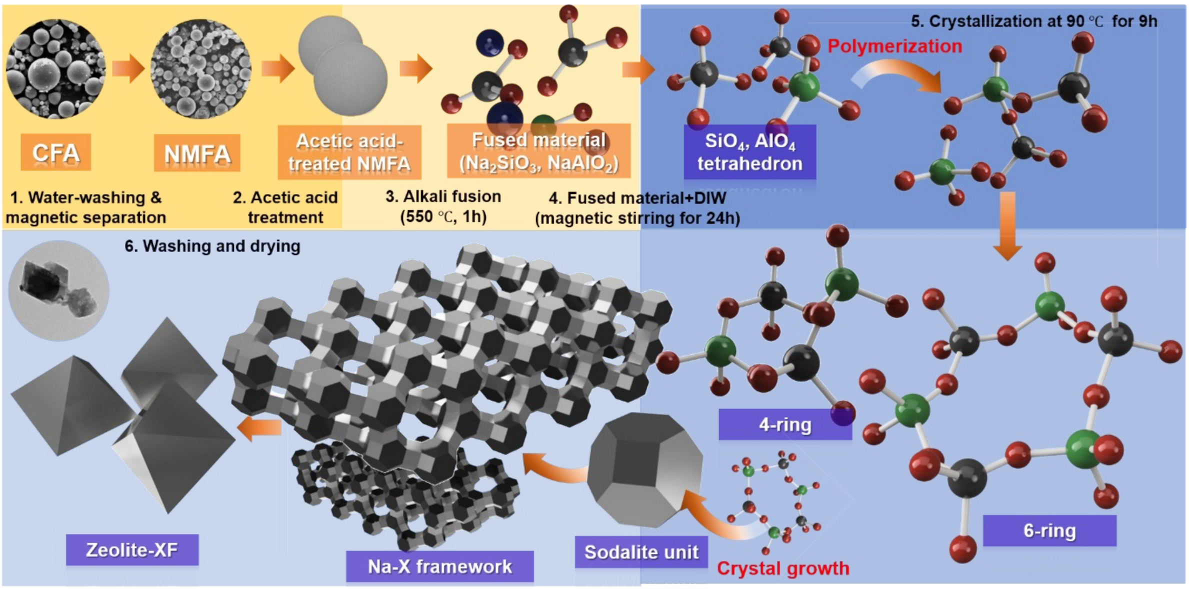

Scheme S1. Preparation of Zeolite-XF from coal fly ash.

Supporting Information

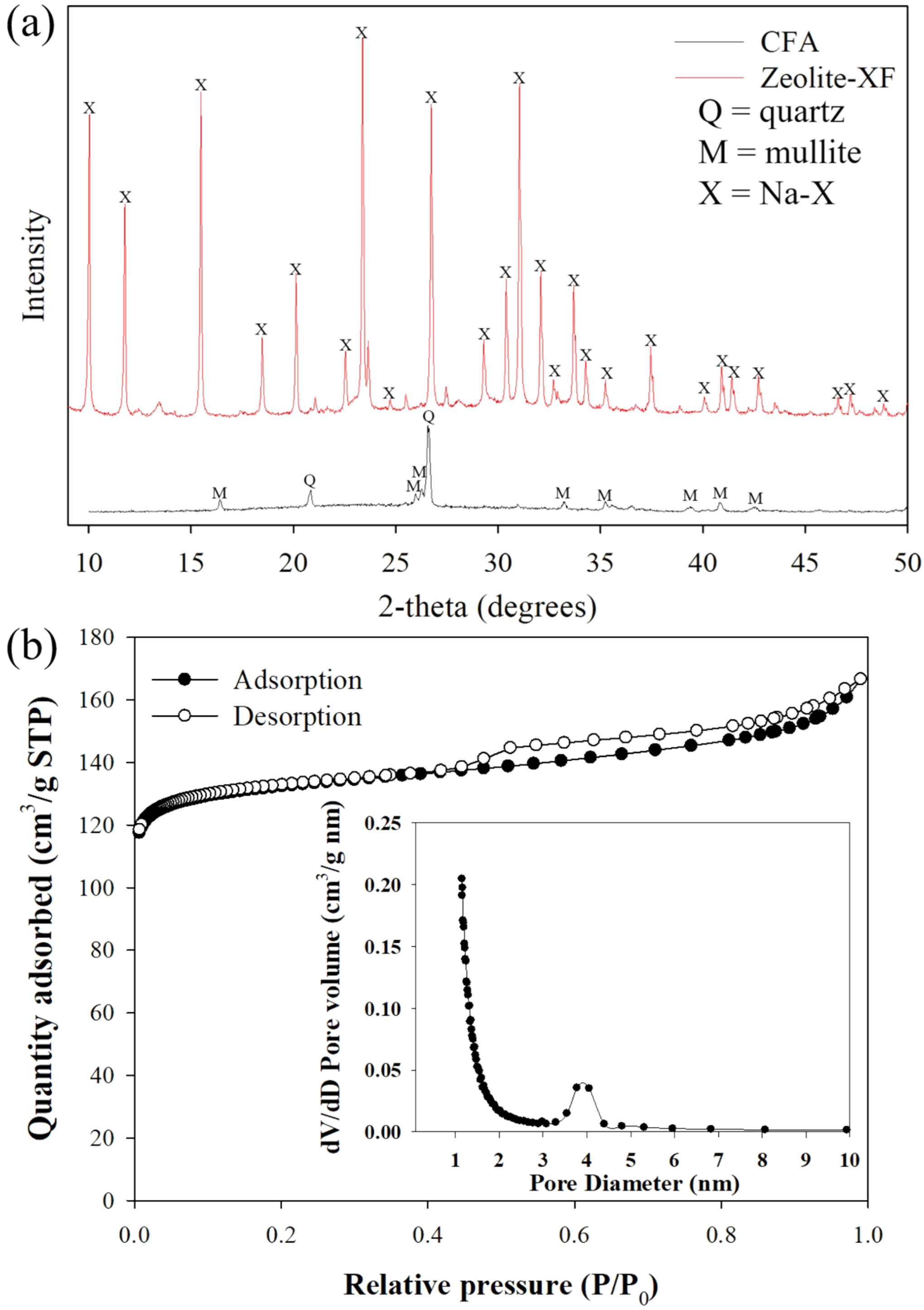

Figure S1. (a) XRD patterns of CFA and Zeolite-XF; Q = quartz, M = mullite, X = Na-X. (b) Isotherm adsorption and desorption of N_2 for Zeolite-XF (inset: pore size distribution of Zeolite-XF).

Supporting Information

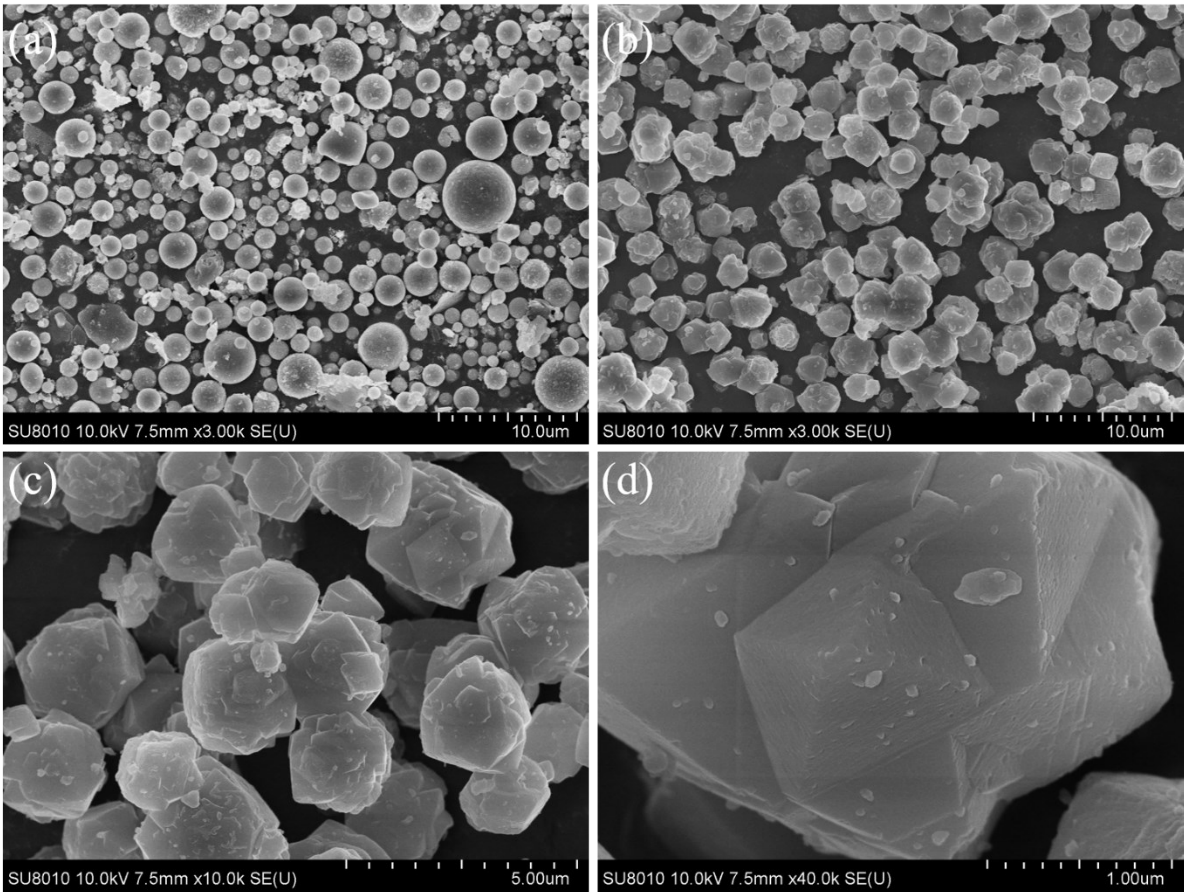

Figure S2. SEM images of (a) NMFA and (b-d) molecular sieves 13X (C-13X, ~2 μm, Sigma-Aldrich Inc., USA).

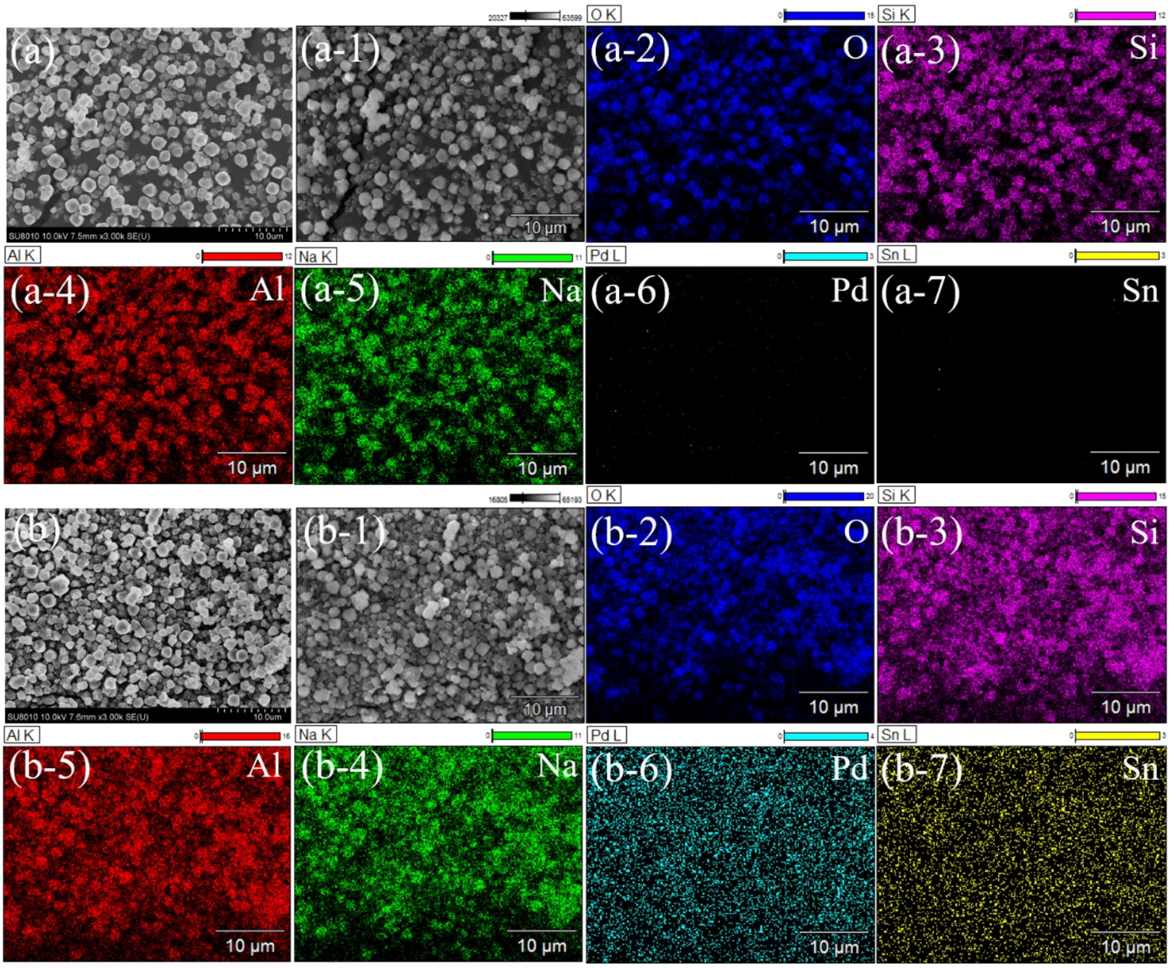

Figure S3. HR-FESEM/EDX analysis of Zeolite-XF (a, a-1), 1.5 wt.% Pd-0.5 wt.% Sn/Zeolite-XF (b, b-1) after activation; EDX electron mapping of O (a-2, b-2), Si (a-3, b-3), Al (a-4, b-4), Na (a-5, b-5), Pd (a-6, b-6), and Sn (a-7, b-7).

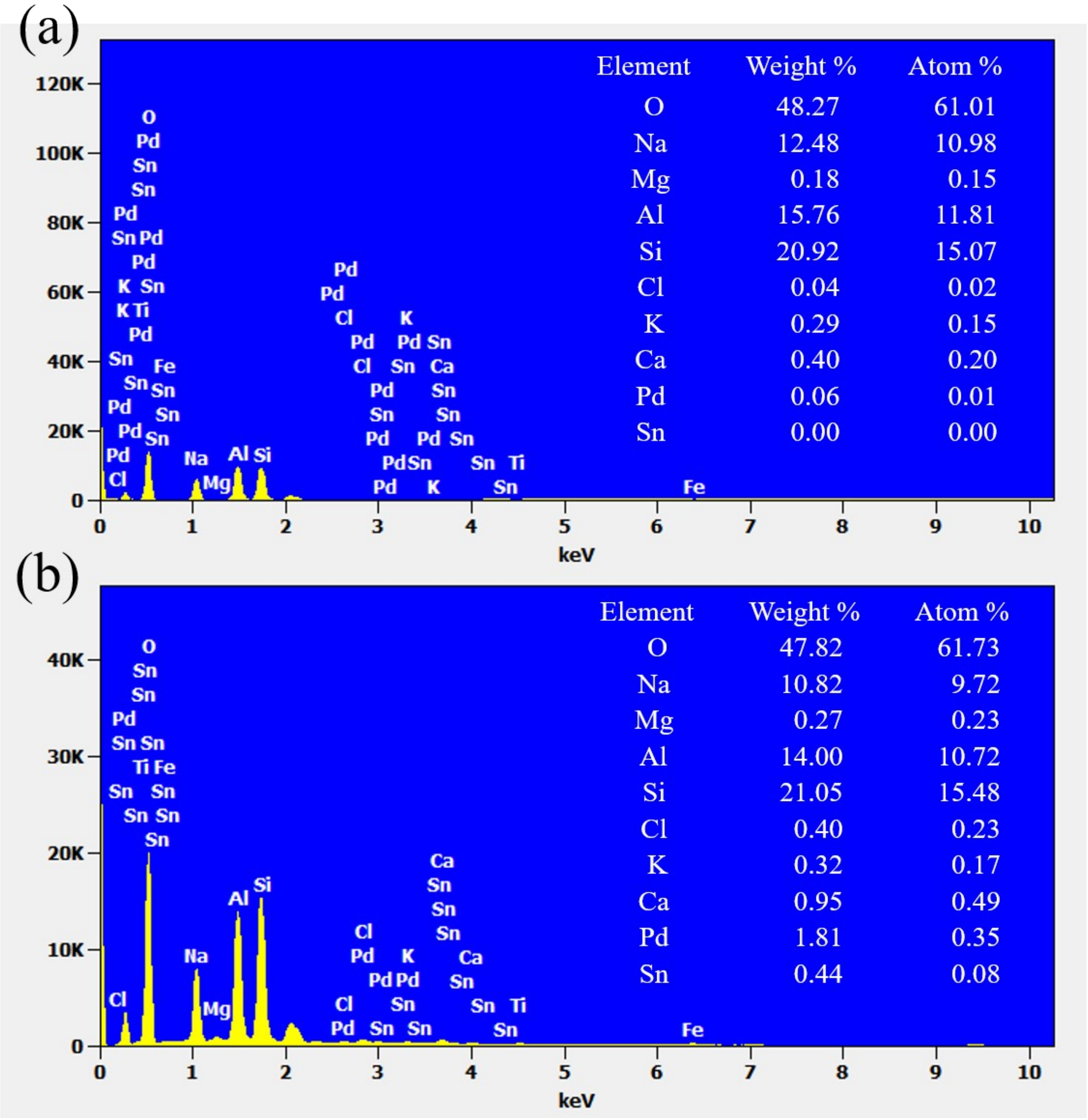

(a)

Element	Weight %	Atom %
O	48.27	61.01
Na	12.48	10.98
Mg	0.18	0.15
Al	15.76	11.81
Si	20.92	15.07
Cl	0.04	0.02
K	0.29	0.15
Ca	0.40	0.20
Pd	0.06	0.01
Sn	0.00	0.00

(b)

Element	Weight %	Atom %
O	47.82	61.73
Na	10.82	9.72
Mg	0.27	0.23
Al	14.00	10.72
Si	21.05	15.48
Cl	0.40	0.23
K	0.32	0.17
Ca	0.95	0.49
Pd	1.81	0.35
Sn	0.44	0.08

Figure S4. EDX spectra of (a) Zeolite-XF, (b) Pd-Sn/Zeolite-XF after activation**.**

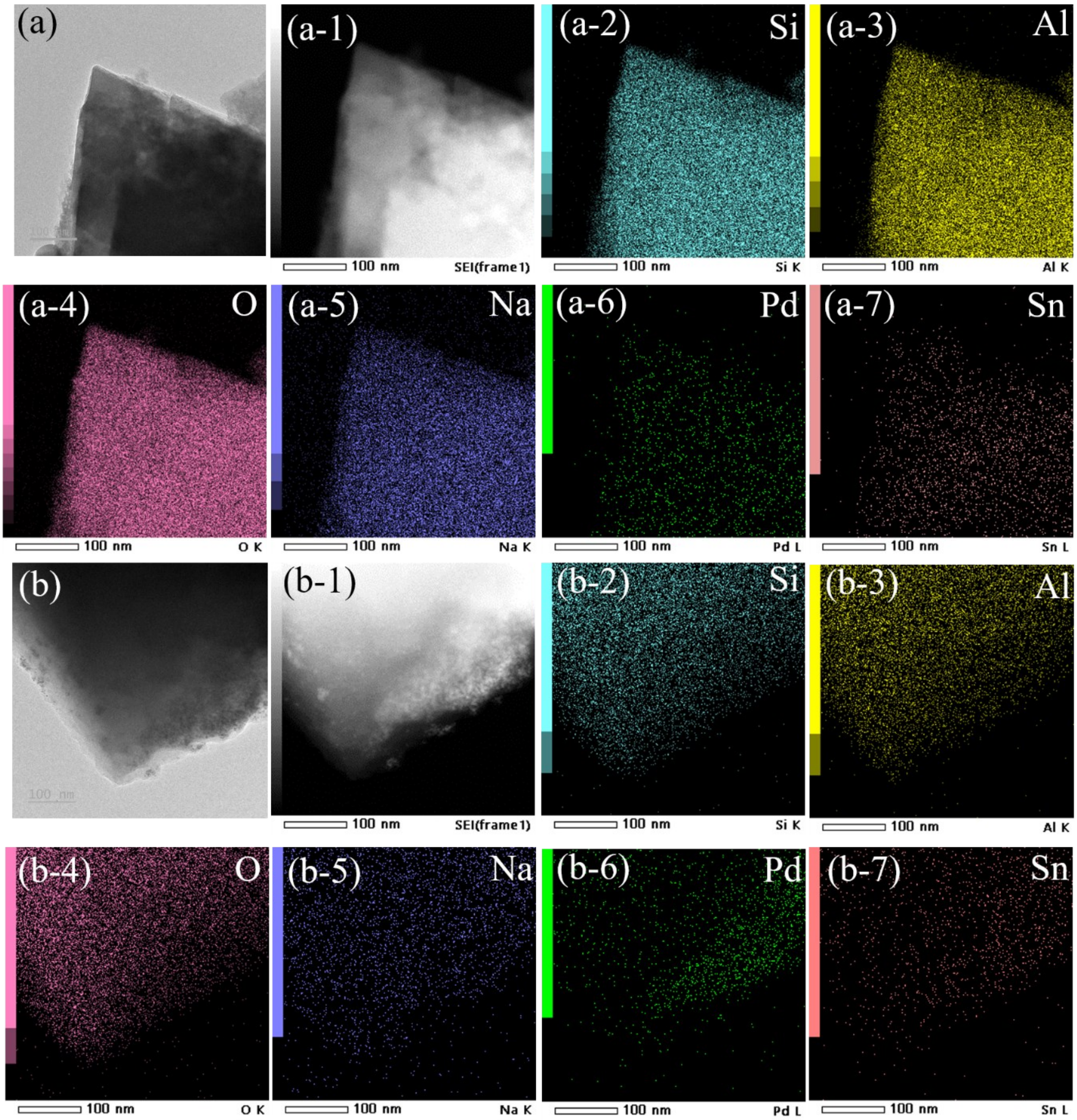

Figure S5. FE-TEM/EDX analysis of Zeolite-XF (a, a-1), and 1.5 wt.% Pd–0.5 wt.% Sn/Zeolite-XF (b, b-1) after activation; EDX electron mapping of Si (a-2, b-2), Al (a-3, b-3), O (a-4, b-4), Na (a-5, b-5), Pd (a-6, b-6), and Sn (a-7, b-7).

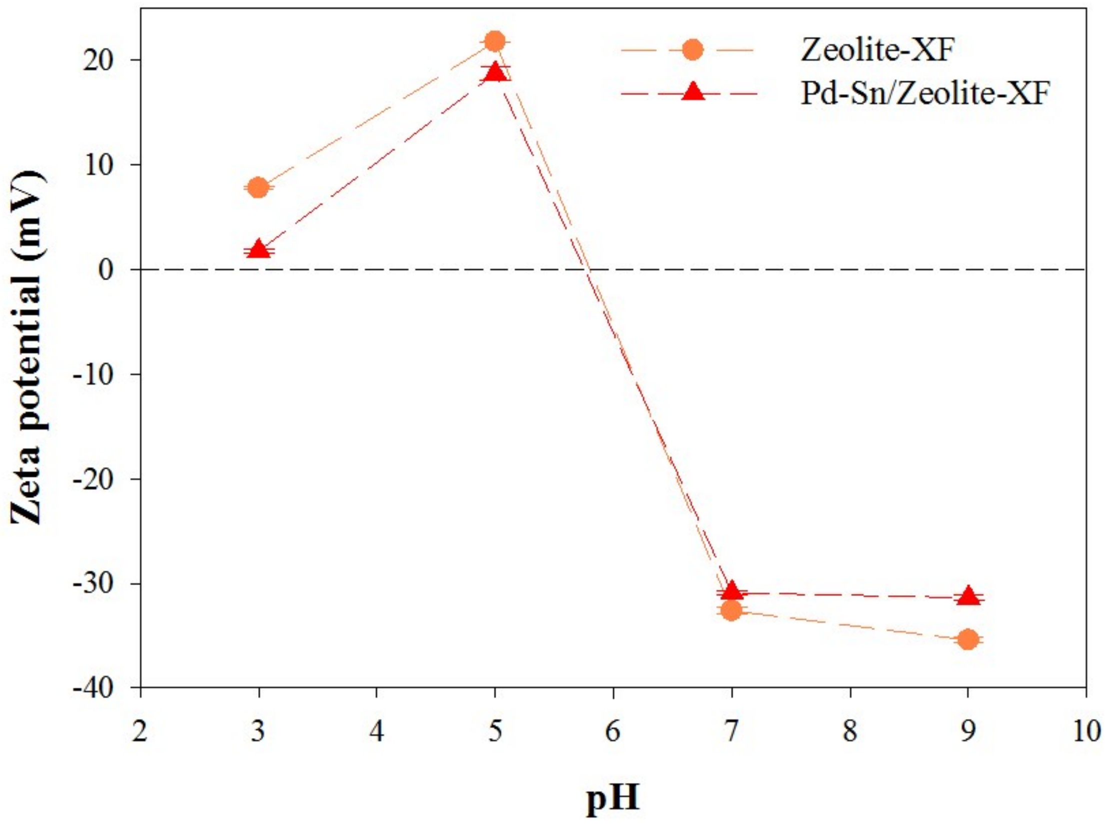

Figure S6. Zeta potential profiles of Zeolite-XF, and Pd-Sn/Zeolite-XF.

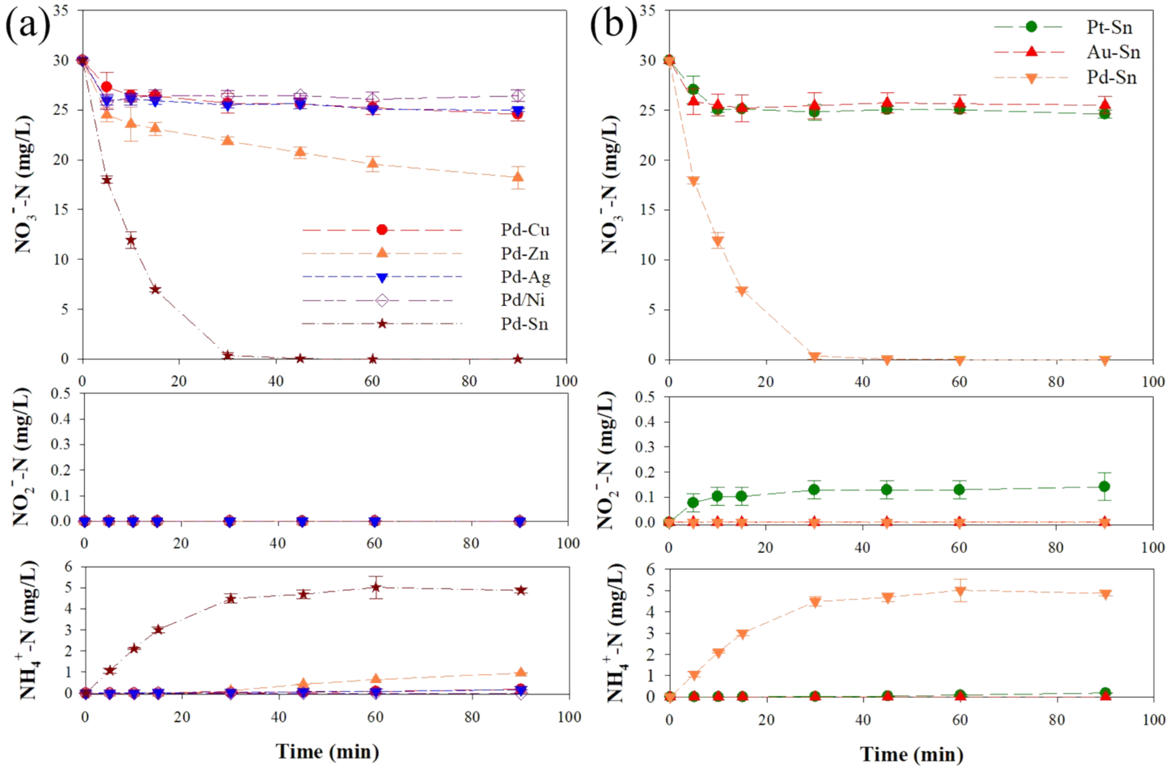

Figure S7. (a) Catalytic NO_3^- reduction by 1.5 wt.% Pd–0.5 wt.% Cu/Zeolite-XF, 1.5 wt.% Pd–0.5 wt.% Zn/Zeolite-XF, 1.5 wt.% Pd–0.5 wt.% Ni/Zeolite-XF, 1.5 wt.% Pd–0.5 wt.% Ag/Zeolite-XF, and 1.5 wt.% Pd–0.5 wt.% Sn/Zeolite-XF. (b) Catalytic NO_3^- reduction by 1.5 wt.% Pt–0.5 wt.% Sn/Zeolite-XF, 1.5 wt.% Au–0.5 wt.% Sn/Zeolite-XF, and 1.5 wt.% Pd–0.5 wt.% Sn/Zeolite-XF. Conditions: NO_3^- loading: 30 mg/L NO_3-N; catalyst loading: 1.25 g/L; H_2 flow rate: 30 mL/min; CO_2 flow rate: 40 mL/min.

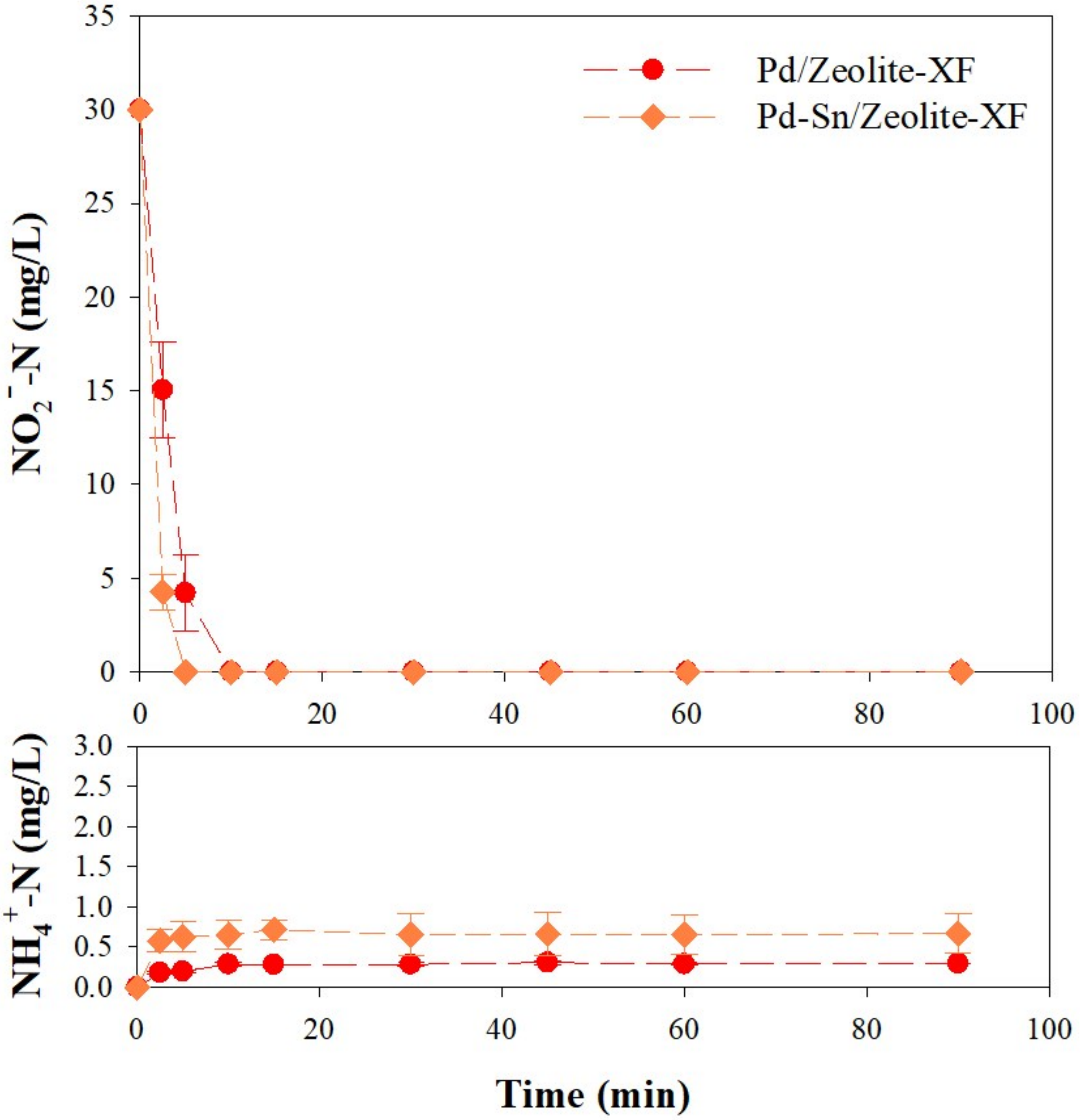

Figure S8. Catalytic NO_2^- reduction by 1.5 wt.% Pd/Zeolite-XF and 1.5 wt.% Pd-0.5 wt.% Sn/Zeolite-XF. Conditions: NO_2^- loading: 30 mg/L NO_2-N; catalyst loading: 1.25 g/L; H_2 flow rate: 30 mL/min; CO_2 flow rate: 40 mL/min.

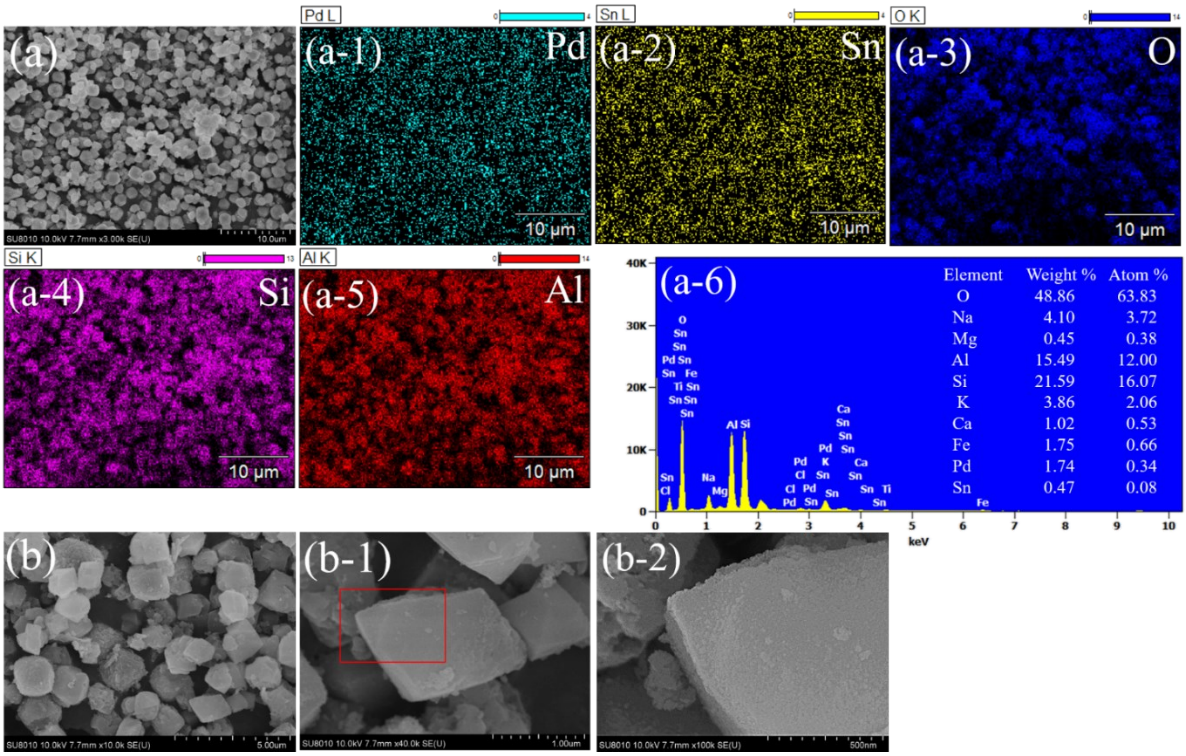

Element	Weight %	Atom %
O	48.86	63.83
Na	4.10	3.72
Mg	0.45	0.38
Al	15.49	12.00
Si	21.59	16.07
K	3.86	2.06
Ca	1.02	0.53
Fe	1.75	0.66
Pd	1.74	0.34
Sn	0.47	0.08

Figure S9. HR-FESEM/EDX analysis of (b, b-1, b-2) 1.5 wt.% Pd-0.5 wt.% Sn/Zeolite-XF after the catalytic reaction; EDX electron mapping of Pd (a-1), Sn (a-2), O (a-3), Si (a-4), Al (a-5), and EDX spectra (a-6).

Supporting Information

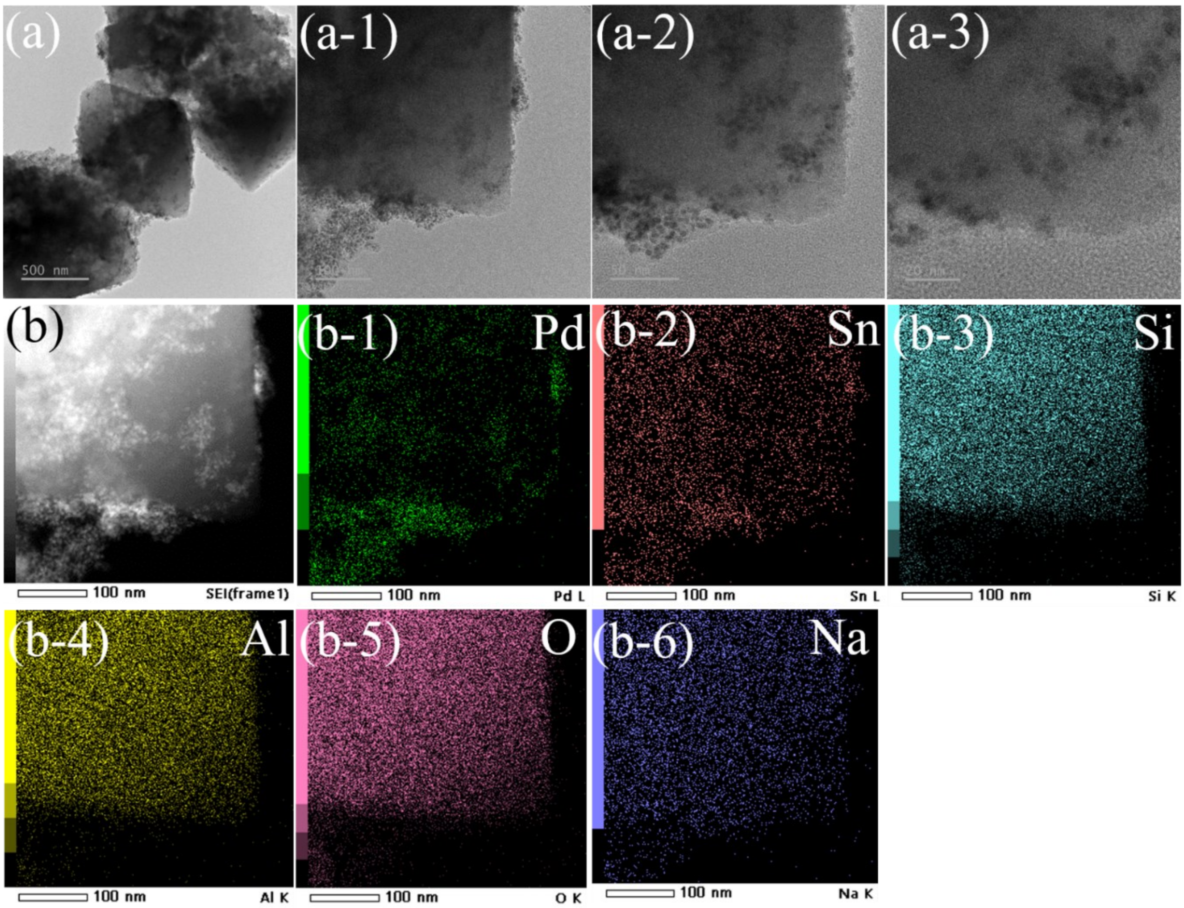

Figure S10. FE-TEM images of (a, a-1, a-2, a-3) 1.5 wt.% Pd-0.5 wt.% Sn/Zeolite-XF after the catlytic reaction; EDX electron mapping of Pd (b-1), Sn (b-2), Si (b-3), Al (b-4), O (b-5), and Na (b-6).

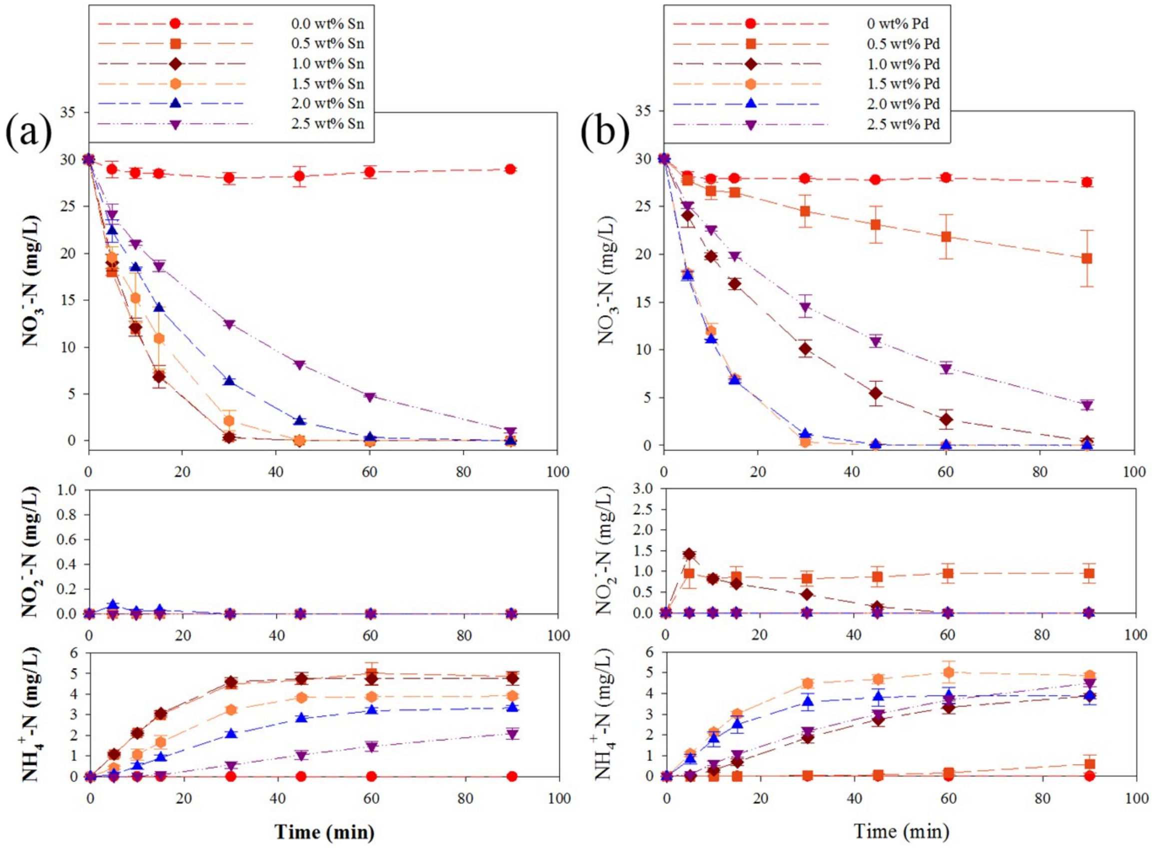

Figure S11. (a) Catalytic NO_3^- reduction by 1.5 wt.% Pd-X wt.% Sn/Zeolite-XF (X = 0, 0.5, 1.0, 1.5, 2.0 and 2.5) (b) Catalytic NO_3^- reduction by X wt.% Pd-0.5 wt.% Sn/Zeolite-XF (X = 0, 0.5, 1.0, 1.5, 2.0 and 2.5). Conditions: NO_3^- loading: 30 mg/L NO_3-N; catalyst loading: 1.25 g/L; H_2 flow rate: 30 mL/min; CO_2 flow rate: 40 mL/min

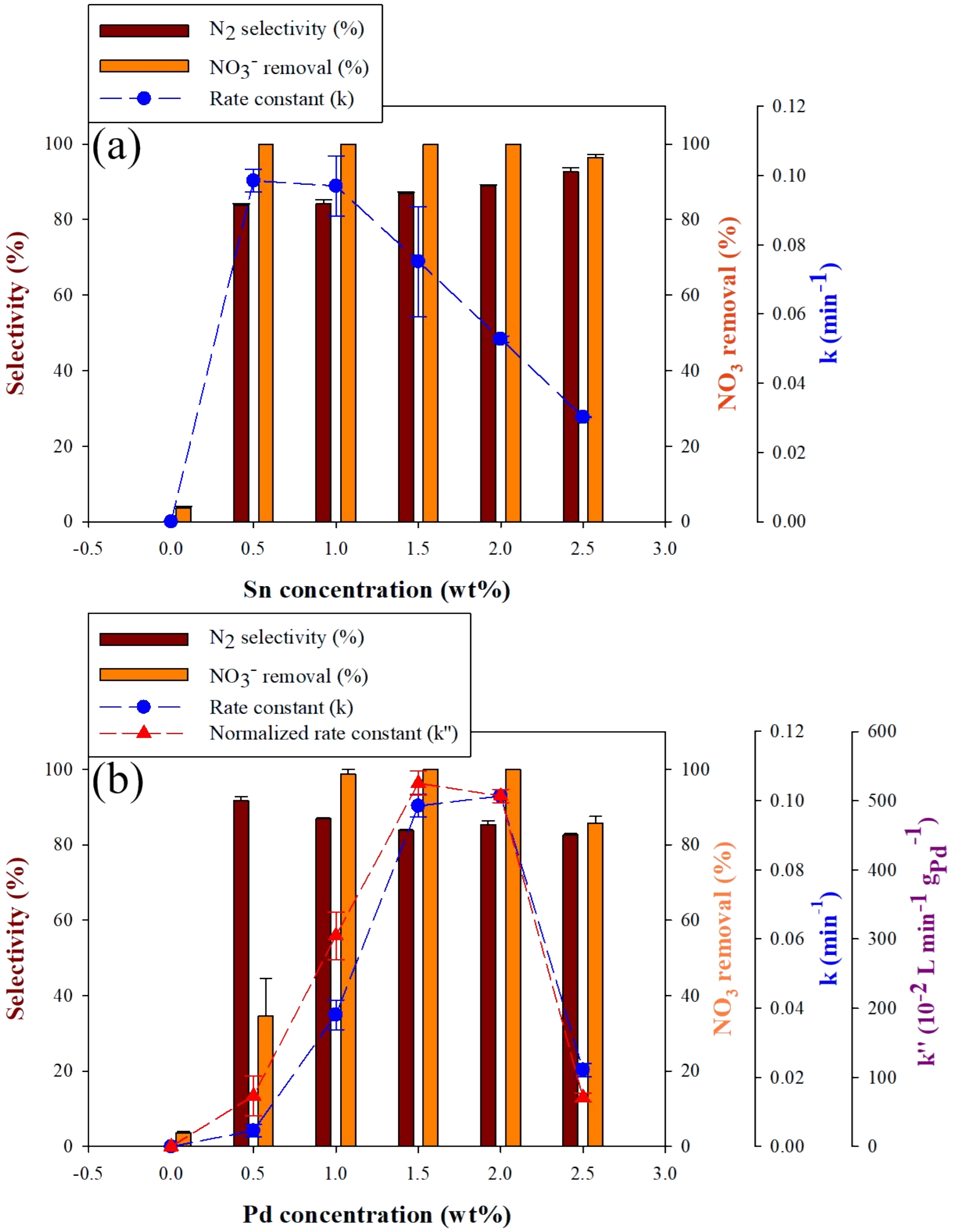

Figure S12 (a) N_2 selectivity, NO_3^- removal, and rate constants (k and k'') by X wt.% Sn-1.5 wt.% Pd/Zeolite-XF (X = 0, 0.5, 1.0, 1.5, 2.0, and 2.5) and (b) 0.5 wt.% Sn-X wt.% Pd/Zeolite-XF (X = 0, 0.5, 1.0, 1.5, 2.0, and 2.5) Conditions: NO_3^- loading: 30 mg/L NO_3-N; catalyst loading: 1.25 g/L; H_2 flow rate: 30 mL/min; CO_2 flow rate: 40 mL/min; reaction time: 90 min.

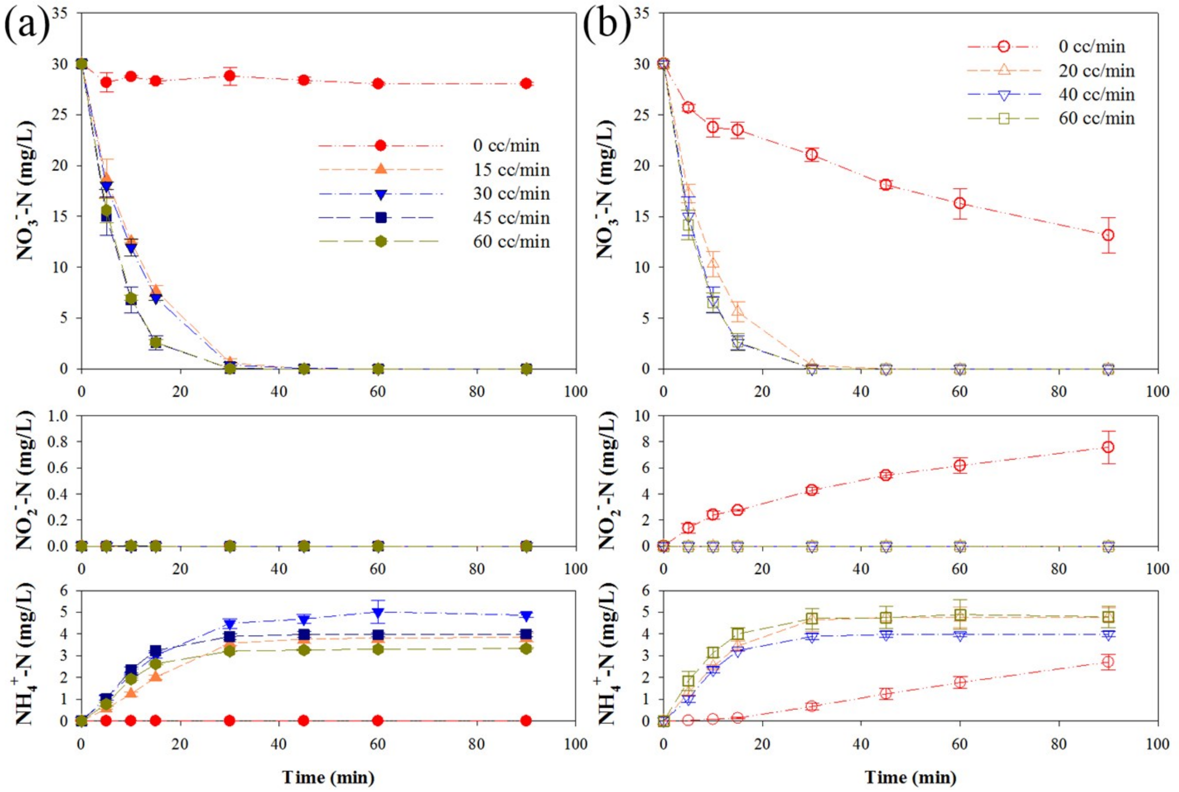

Figure S13. (a) Catalytic NO_3^- reduction by 1.5 wt.% Pd-0.5 wt.% Sn/Zeolite-XF at different H_2 flow rates (0, 15, 30, 45, 60 cc/min). Conditions: NO_3^- loading: 30 mg/L NO_3-N; catalyst loading: 1.25 g/L; CO_2 flow rate: 40 mL/min. (b) Catalytic NO_3^- reduction by 1.5 wt.% Pd-0.5 wt.% Sn/Zeolite-XF at different CO_2 flow rates (0, 20, 40, 60 cc/min). Conditions: NO_3^- loading: 30 mg/L NO_3-N; catalyst loading: 1.25 g/L; H_2 flow rate: 45 mL/min.

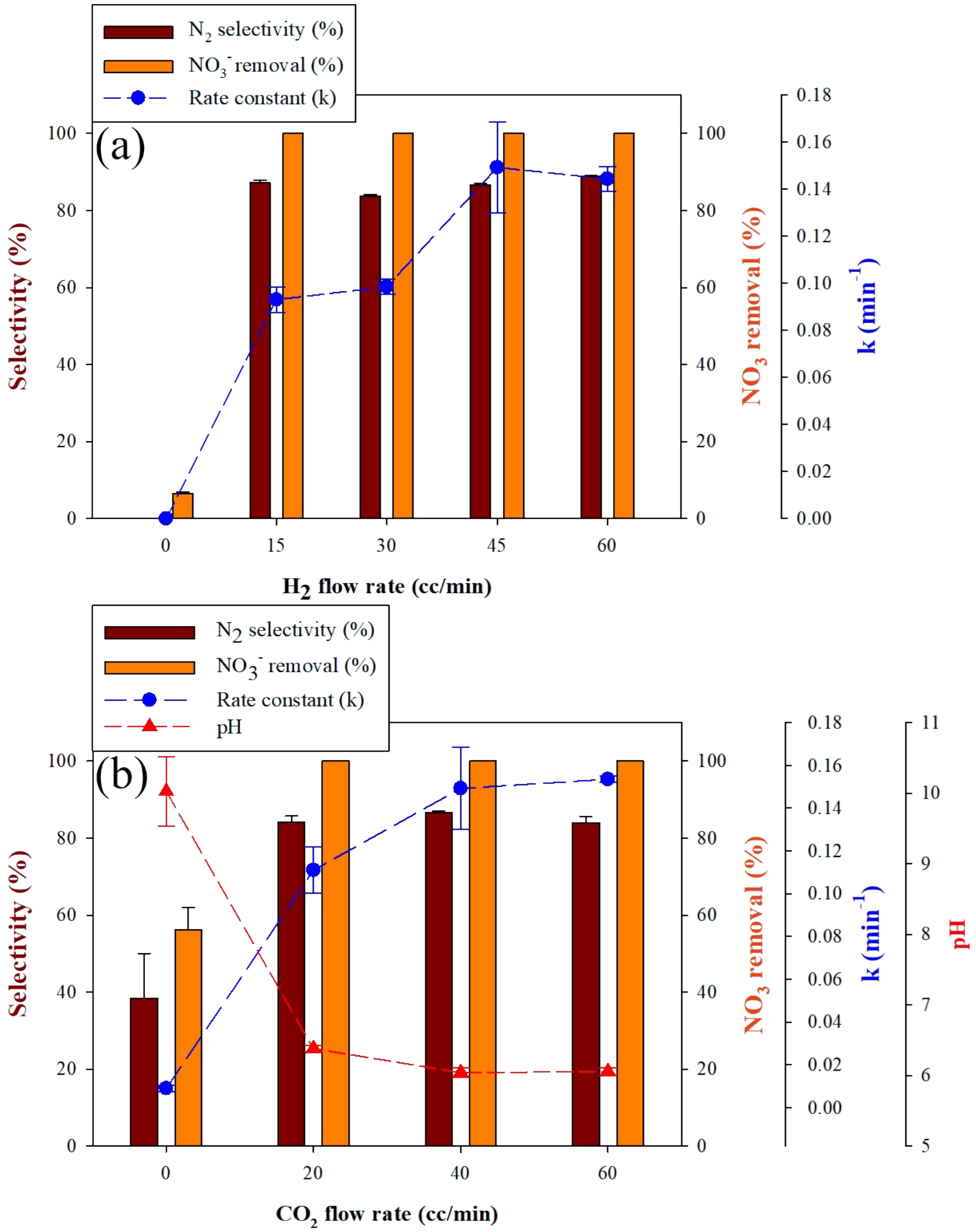

Figure S14. (a) N_2 selectivity, NO_3^- removal and rate constant (k) by 1.5 wt.% Pd-0.5 wt.% Sn/Zeolite-XF at different H_2 flow rates. Conditions: NO_3^- loading: 30 mg/L NO_3-N; catalyst loading: 1.25 g/L; CO_2 flow rate: 40 mL/min; reaction time: 90 min. (b) N_2 selectivity and NO_3^- removal by 1.5 wt.% Pd-0.5 wt.% Sn/Zeolite-XF at different CO_2 flow rates. Conditions: NO_3^- loading: 30 mg/L NO_3-N; catalyst loading: 1.25 g/L; H_2 flow rate: 45 mL/min; reaction time: 90 min.

Supporting Information

Effect of experimental factors on NO_3^- reduction and byproduct selectivity: Data description and discussion for Figure S12-S15

Figures S11(a) and 12(a) show the removal kinetics of NO_3^-, the selectivity towards NO_2^- and N_2, and rate constant (k) of 1.5% Pd-Sn/Zeolite-XF catalyst at different Sn loadings (0, 0.5, 1.0, 1.5, 2.0, 2.5 wt.%) in 90 min. We observed insignificant NO_3^- removal (3.6%) by 1.5 wt.% Pd-0 wt.% Sn/Zeolite-XF, confirming that monometallic Pd/Zeolite-XF alone could not proceed the NO_3^- reduction owing to its poor affinity for NO_3^-.[5–7] However, almost complete NO_3^- removal was achieved by all Sn loadings from 0.5 to 2.5 wt.% within 90 min. The k value decreased with increasing the Sn loading (from $9.85 \pm 0.32 \times 10^{-2}$ min^{-1} at 0.5 wt.% Sn, to $3.01 \pm 0.02 \times 10^{-2}$ min^{-1} at 2.5 wt.% Sn), implying that an increase in Sn loading beyond 0.5 wt.% negatively affected the reactivity of Pd-Sn/Zeolite-XF by covering the active surface area of Pd particles.[8] However, N_2 selectivity dramatically increased with increasing the Sn loading (from 83.8% at 0.5 wt.% Sn, to 92.8% at 2.5 wt.% Sn) owing to the decrease in number of H_{ads} on Pd sites by blocking corners and edges of Pd particles, leading to higher N:H_{ads} ratio and formation of more N_2 than NH_4^+. The accumulation of NO_2^- was not observed during all experiments, implying that the increase in Sn loading up to 2.5 wt.% still induced the instantaneous reduction of NO_2^- by H_{ads}-Pd of Pd-Sn/Zeolite-XF in this study. Hence, 0.5 wt.% Sn loading was fixed as the optimal level to provide complete NO_3^- removal with the highest reactivity and good N_2 selectivity.

Figures S11(b) and 12(b) show the NO_3^- removal, NO_2^- and N_2 selectivity, and rate constant by Pd-Sn/Zeolite-XF catalyst at different levels of Pd loading (0, 0.5, 1.0, 1.5, 2.0, 2.5 wt.%) in 90 min. No significant removal of NO_3^- (3.6%) was observed at 0 wt.% of Pd loading, confirming that adsorption and reduction of NO_3^- on the surface of monometallic Sn/Zeolite-XF alone was almost negligible. The increase in Pd loading from 0.5 wt.% to 2.0 wt.% dramatically enhanced NO_3^- removal (from 34.7% at 0.5 wt.% Pd to 100% at 2.0 wt.% Pd).

But, there was decrease in NO_3^- removal rate at 2.5 wt.% of Pd (85.8%). Similar trends were observed for the k and k'' value, showing the volcano shape and reaching the maximum value (5.25 ± 0.17 $L\cdot min^{-1}\ g_{Pd}^{-1}$) at 1.5 wt.% Pd followed by a drop at 2.5 wt.% Pd (0.71 ± 0.06 $L\cdot min^{-1}\ g_{Pd}^{-1}$). The experimental results demonstrated that the increase in Pd loading from 0.5 to 1.5 wt.% accelerated the activation of H_2 molecules on the reactive sites (i.e., edge, corner, and terrace) of Pd nanoparticles, resulting in enhanced reduction of NO_3^- to NO_2^- ($NO_3^- + Sn^0 \rightarrow NO_2^- + SnO$, $NO_3^- + SnO \rightarrow NO_2^- + SnO_2$) with continuous and swift rejuvenation of SnO_2 and SnO to Sn^0 by increased hydrogen spillover from a large number of active sites of metallic Pd. The results also illustrated that NO_2^- selectivity decreased with the increase of Pd loading from 0.5 to 1.5 wt.%, indicating the enhancement of NO_2^- reduction to N_2 or NH_4^+ over the surface of Pd (Fig.S9(b)). Furthermore, Pd loading above 2.0 wt.% damaged the catalytic reactivity of Pd-Sn/Zeolite-XF due probably to the agglomeration of Pd nanoparticles and overlapping of Sn particles, resulting in the decrease of reactive sites of both Pd and Sn nanoparticles.[2] The N_2 selectivity decreased from 91.7 % to 83.8% with increasing Pd loading from 0.5 to 1.5 wt.% and reached a plateau (83.5-86%) from 1.5 to 2.0 wt.%. This evidence can suggest that the increase of Pd loading led to the increase in reactive H_{ads} which lowers the $N:H_{ads}$ ratio, facilitating N-H recombination to form NH_4^+. However, this phenomenon was not observed above 1.5 wt.% Pd, showing no further decrease of N_2 selectivity. It is because fast oxidation of Sn^0 led to the prompt consumption of surplus H_{ads} on Pd sites for its rejuvenation, and then NO_2^- load on Pd sites increased due to fast reduction of NO_3^- by swiftly regenerated Sn^0 and SnO.[7] This condition created higher $N:H_{ads}$ on Pd sites under constant and limited supply of H_2 (30 cc/min), resulting in ultimately high selectivity towards N_2 more than 83.5%. Therefore, the optimal proximity of Pd and Sn was determined optimal Pd loading at 1.5 wt.% owing to the highest reactivity of the bimetallic catalyst and good N_2 selectivity.

Figures S13(a) and S14(a) show the removal kinetics of NO_3^-, the selectivity towards NO_2^- and N_2, and the rate constant (*k*) of the 1.5 wt.% Pd–0.5 wt.% Sn/Zeolite-XF catalyst at different H_2 flow rates (0, 15, 30, 45, and 60 cc/min) with CO_2 (40 cc/min). The main findings in the H_2 flow rate experiments were that (i) no significant removal of NO_3^- was observed without H_2 injection, showing an essential prerequisite role of H_2 for continuous NO_3^- reduction by Pd–Sn/Zeolite-XF, and (ii) increasing the H_2 flow rate to 45 cc/min tended to increase the removal rate because of the enhanced activation of H_2 molecules on the Pd sites as the H_2 flow rate increased.[9] Interestingly, we observed relatively constant high N_2 selectivity (83.5−89.0%), which contradicts the findings for Pd–Cu and Pd–Sn bimetallic catalysts in recent studies.[9,10] In general, the N_2 selectivity of Pd-based bimetallic catalysts decreased with increasing H_2 flow rate owing to the lower N:H_{ads} ratio. However, this phenomenon was not observed in this study because of the presence of highly dispersive bimetallic ensembles on the surface of the Zeolite-XF, with optimized proximity of Pd and Sn and a large number of active metallic sites. Indeed, this condition accelerated the utilization of H_{ads} from Pd for regeneration of SnOx to Sn^0 and fast reduction of NO_2^- to final products, which could offset escalating H_2 activation on Pd sites and maintain a suitable N:H ratio for high N_2 selectivity even at a high H_2 supply (~60 cc/min). Thus, no detection of NO_2^- was observed in all H_2 flow rates. Considering the removal kinetics, N_2 selectivity, and amount of metal, we selected the optimal H_2 flow rate of 45 cc/min for further study of the effect of CO_2 and recycling tests.

Figures S13 (b) and S14(b) show the removal kinetics of NO_3^-, byproduct selectivity, and pH after reaction by 1.5 wt.% Pd–0.5 wt.% Sn/Zeolite-XF at different CO_2 flow rates (0, 20, 40, and 60 cc/min). In the case without a CO_2 supply, we observed low NO_3^- removal (56.2%) with 45.5% and 38.4% NO_2^- and N_2 selectivity, respectively. The decreases in both NO_3^- removal and NO_2^- reduction may have been caused by the pH increase to 10.0 (Figure S14(b)) owing to the accumulation of OH^- generated from (i) the conversion of NO_2^- into N_2 or NH_4^+

($4NO_2^- + 18H_{ads}\text{-}Pd^0 \rightarrow Pd^0 + N_2 + 2NH_4^+ + 6OH^- + 2H_2O$) and (ii) the continuous rejuvenation of Sn species by oxygen abstraction in the Pd–Sn bimetallic system ($3H_{ads}\text{-}Pd^0 + SnO + SnO_2 \rightarrow 2Sn^0 + Pd^0 + 3OH^-$).[5] An excessive amount of OH^- could cover the active metallic sites and negatively affect the affinities of NO_3^- and NO_2^- via electrostatic repulsion, [9] resulting in the obstruction of consecutive reduction steps of NO_3^- and build-up of NO_2^- as the reaction proceeded. Thus, to avoid this inhibitory effect, continuous consumption of OH^- using an appropriate buffering system is essential, such as the CO_2 supply used in this study. Indeed, Figure S14(b) shows that the pH after reaction significantly decreased from 10.0 to 5.8−6.0 as the CO_2 flow rate increased from 0 to 60 cc/min. Furthermore, all cases showed complete removal of NO_3^- (100%) and high N_2 selectivity (83−87%), signifying that the buffering effect of CO_2 was important for the efficient and sustainable catalytic reduction of NO_3^-. Based on the results of parametric studies, we obtained the fastest reduction kinetics (8.0 ± 1.0 $L\cdot min^{-1}\ g_{Pd}^{-1}$) with high N_2 selectivity (86.7%) under the optimal conditions (i.e., 1.5% Pd–0.5% Sn/Zeolite-XF at a 45 cc/min H_2 flow rate and a 40 cc/min CO_2 flow rate (Table S3)).

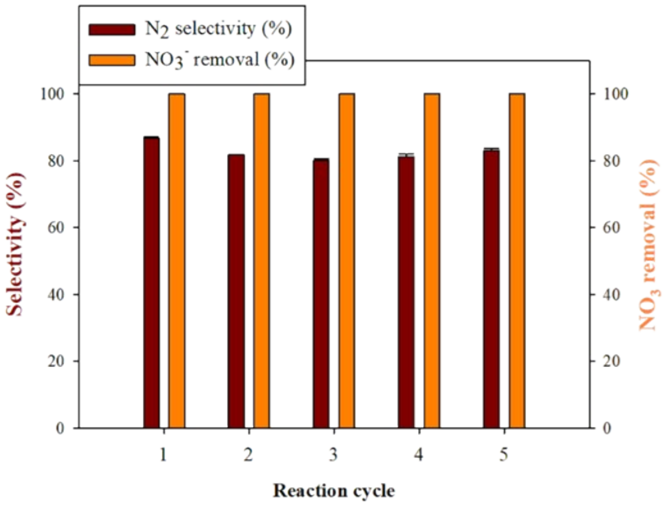

Figure S15. N_2 selectivity and NO_3^- removal rate by 0.5 wt.% Sn–1.5 wt.% Pd/Zeolite-XF during five repeated cycles. Conditions: NO_3^- loading: 30 mg/L NO_3^--N; catalyst loading: 1.25 g/L; H_2 flow rate: 45 mL/min; CO_2 flow rate: 40 mL/min; calcination temperature: 350 °C; reaction time: 90 min.

Supporting Information

Table S1. Oxidation states of Sn before/after activation and after reaction

	Sn^0 (%)	**Sn^{2+} (%)**	**Sn^{4+} (%)**
Before activation	0	15.3	84.7
After activation	32.7	8.8	58.5
After reaction	30.4	2.0	67.6

Supporting Information

Catalyst	Pollutant	H_2 flow rate (cc/min)	CO_2 flow rate (cc/min)	k ×$\mathbf{10^{-2}}$ (min^{-1})	k’ ×$\mathbf{10^{-2}}$ (min^{-1} g_{cat}^{-1})	k’’ ×$\mathbf{10^{-2}}$ (L min^{-1} g_{pd}^{-1})	Removal rate (%)	N_2 selectivity (%)
1.5% Pd/Zeolite-XF	30 mg L^{-1} NO_3-N	30	40	–	–	–	3.6 ± 0.4	–
	30 mg L^{-1} NO_2-N	30	40	33.7 ± 6.1	134.6 ± 24.6	1794.7 ± 327.3	100	99.2 ± 0.2
1.5% Pd-0.5% Sn/Zeolite-XF	30 mg L^{-1} NO_3-N	30	40	9.9 ± 0.3	39.4 ± 1.3	525.3 ± 17.5	100	83.8 ± 0.4
	30 mg L^{-1} NO_2-N	30	40	80.1 ± 8.2	320.3 ± 32.9	4270.4 ± 434.0	100	97.8 ± 0.8

Table S2. Kinetics and N_2 selectivity of monometallic and bimetallic catalyst for nitrate and nitrite reduction

$[NO_3^-$-N$]_0$ (mg/L)	Catalyst (X% Pd-X% promoter metal/Support)	[Catalyst] (g/L)	H_2 flow rate	Buffer	*k* ×10^{-2} (min^{-1})	*k*′ ×10^{-2} (min^{-1} g_{cat}^{-1})	*k*″ ×10^{-2} (L.min^{-1} g_{Pd}^{-1})	NO_3^- removal (%)	N_2 selectivity (%)	NH_4^+ selectivity (%)	TOF ×10^{-3} (sec^{-1})	Ref.
30	1.5% Pd–0.5% Sn/Al_2O_3	1.25	30 mL/min	CO_2 (40 mL/min)	1.7	6.8	90.7	73.3	67.3	32.7	NA	This study
22.6	4% Pd–1% Cu/Al_2O_3	2.00	0.15 atm	0.2 M HCl	13.0	6.5	145.9	100	82.3	17.7	NA	[14]
22.6	4.4% Pd–1.21% Sn/Al_2O_3	0.48	90 mL/min	CO_2 (90 mL/min)	1.2	3.5	58.3	100	88	12	NA	[15]
30	1.5% Pd–0.5% Sn/SiO_2	1.25	30 mL/min	CO_2 (40 mL/min)	1.3	5.2	69.3	68.3	69.2	30.8	NA	This study
22.6	5% Pd–1.25% Cu/amorphous alumina-silica (ASA)	0.80	200 mL/min	CO_2 (100 mL/min)	6.5	16.1	161.3	100	90.2	9.8	NA	[16]
22.6	2% Pd–1% Cu/TiO_2	1.00	60 mL/min	CO_2 (NA)	6.7	66.6	333.0	100	76	19	NA	[17]
50	3% Pd–1% Cu/TiO_2	1.00	100 mL/min	MES buffer	4.8	24.0	160.0	100	50.2	49.7	NA	[18]
30	2.8% Pd–1.6% Cu/α-Fe_2O_3	1.25	30 mL/min	CO_2 (40 mL/min)	3.3	13.1	93.3	96.4	70	30	1.5	[19]
40	0.3% Pd–0.5% Cu/Iron	7.69	NA	NA	0.7	1.3	29.0	91.5	29.6	65.6	NA	[20]
22.6	2% Pd–0.4% Cu/activated carbon (NC80)	1.00	333 mL/min	CO_2 (333 mL/min)	3.7	3.7	186.5	74.4	51.3	48.3	NA	[21]
22.6	2% Pd–1% Cu/activated carbon (ACo)	0.51	200 Nc m^3/min	CO_2 (200Ncm^3/min)	0.3	0.8	61.2	59	60	40	NA	[22]
30	1.6% Pd–2.2% Sn/NBeta	2.50	30 mL/min	CO_2 (60 mL/min)	19.1	76.4	477.3	100	80.8	19.2	11.13	[6]
30	1.6% Pd–1.6% Sn/NZSM-5	1.25	30 mL/min	CO_2 (60 mL/min)	9.4	37.6	470	100	90.7	9.3	8.7	[9]
30	1.6% Pd–1% Sn/red mud	1.25	30 mL/min	CO_2 (60 mL/min)	11.6	46.3	578.5	100	88.7	11.3	NA	[7]

Table S3. Comparison of the reactivity and selectivity of various bimetallic catalysts for NO_3^- reduction under different experimental conditions.

30	2.2% Pd–2.2% Sn/Kaolinite	2.50	30 mL/min	CO_2 (60 mL/min)	18.2	72.4	329.1	100	71	29	10.4	[23]
30	1.5% Pd–1.5% Sn/Zeolite-X&HS15	1.25	30 mL/min	CO_2 (40 mL/min)	5.5	21.9	292.2	100	88.1	11.9	NA	[5]
30	1.5% Pd–1.5% Sn/Zeolite-X&A&HS12	1.25	30 mL/min	CO_2 (40 mL/min)	4.1	16.4	218.7	100	88.5	11.5	NA	[5]
30	1.5% Pd–0.5% Sn/Zeolite-XF	1.25	45 mL/min	CO_2 (40 mL/min)	14.9	59.7	795.7	100	86.7	13.3	43.1	This study
30	1.5% Pd–0.5% Sn/Zeolite-XF	1.25	45 mL/min	CO_2 (60 mL/min)	15.4	61.4	818.7	100	84.0	16.0	43.2	This study

Table S4. ICP-MS results showing the leaching of elements after reduction of nitrate or nitrite (30 mg L^{-1} NO_x-N) by Pd-Sn bimetallic catalysts (1.25 g/L) for 90 min. nd=non-detectable (< MDL) Method Detection Limit (MDL, µg/L); Cr = 0.396, As = 0.006, Pd = 0.038, Sn = 0.298, Pb = 0.004, Mn = 0.033

Catalyst	**Cycle**	**Pollutant**	**H_2 flow rate (cc/min)**	**CO_2 flow rate (cc/min)**	Element					
					Pd (µg/L)	**Sn** (µg/L)	**Cr** (µg/L)	**Mn** (µg/L)	**As** (µg/L)	**Pb** (µg/L)
1.5% Pd-0.5% Sn//Zeolite-XF	1	30 mg L^{-1} NO_3-N	45	40	nd	nd	nd	nd	nd	nd
	1		30	40	nd	nd	nd	nd	nd	nd
	1	30 mg L^{-1} NO_2-N	30	40	nd	nd	nd	nd	nd	nd
	1	23.1 ± 0.3 mg L^{-1} NO_3-N (groundwater)	45	40	nd	nd	nd	nd	nd	nd
1.5% Pd-0.5% Sn/Zeolite-XF (recycled)	2	30 mg L^{-1} NO_3-N	45	40	nd	nd	nd	nd	nd	nd
	3		45	40	nd	nd	nd	nd	nd	nd
	4		45	40	nd	nd	nd	nd	nd	nd
	5		45	40	nd	nd	nd	nd	nd	17.9 ± 4.7

Table S5. Concentrations of the components in groundwater used in this study.

Ions	**Concentration (mg/L)**
Cl^-	85.46 ± 0.62
NO_3^-	102.32 ± 1.48
SO_4^{2-}	49.66 ± 1.34
Na^+	43.09 ± 1.15
NH_4^+	0.086 ± 0.012
K^+	0.59 ± 0.04
Mg^{2+}	5.80 ± 0.87
Ca^{2+}	41.93 ± 5.34

Supporting Information

References

1 J. M. Lim, J. Park, J. T. Park and S. Bae, *J. Ind. Eng. Chem.*, 2018, **71**, 378–386.

2 J. Park and S. Bae, *J. Hazard. Mater.*, , DOI:10.1016/j.jhazmat.2019.02.105.

3 K. Ojha, N. C. Pradhan and A. N. Samanta, *Bull. Mater. Sci.*, 2004, **27**, 555–564.

4 J. Jung, S. Bae and W. Lee, *Appl. Catal. B Environ.*, 2012, **127**, 148–158.

5 J. Park, Y. Hwang and S. Bae, *J. Hazard. Mater.*, 2019, **374**, 309–318.

6 S. Hamid, M. A. Kumar, J. Han, H. Kim and W. Lee, *Green Chem.*, 2017, **19**, 853–866.

7 S. Hamid, S. Bae and W. Lee, *Chem. Eng. J.*, 2018, **348**, 877–887.

8 J. Hirayama and Y. Kamiya, *Catal. Sci. Technol.*, 2018, **8**, 4985–4993.

9 S. Hamid, M. A. Kumar and W. Lee, *Appl. Catal. B Environ.*, 2016, **187**, 37–46.

10 S. Jung, S. Bae and W. Lee, *Environ. Sci. Technol.*, 2014, **48**, 9651–9658.

11 J. Martínez, A. Ortiz and I. Ortiz, *Appl. Catal. B, Environ.*, 2017, **207**, 42–59.

12 B. P. Chaplin, E. Roundy, K. A. Guy, J. R. Shapley and C. I. Werth, *Environ. Sci. Technol.*, 2006, **40**, 3075–3081.

13 Y. Wang, Y. Sakamoto and Y. Kamiya, *Appl. Catal. A Gen.*, 2009, **361**, 123–129.

14 Y. X. Chen, Y. Zhang and G. H. Chen, *Water Res.*, 2003, **37**, 2489–2495.

15 J. Sá, D. Gasparovicova, K. Hayek, E. Halwax, J. A. Anderson and H. Vinek, *Catal. Letters*, 2005, **105**, 209–217.

16 Y. Xie, H. Cao, Y. Li, Y. Zhang and J. C. Crittenden, *Environ. Sci. Pollut. Res.*, 2011, **45**, 4066–4072.

17 W. Gao, N. Guan, J. Chen, X. Guan, R. Jin, H. Zeng, Z. Liu and F. Zhang, *Appl. Catal. B Environ.*, 2003, **46**, 341–351.

18 S. Bae, J. Jung and W. Lee, *Chem. Eng. J.*, 2013, **232**, 327–337.

19 S. Jung, S. Bae and W. Lee, *Environ. Sci. Technol.*, 2014, **48**, 9651–9658.

20 Y. H. Liou, C. J. Lin, S. C. Weng, H. H. Ou and S. L. Lo, *Environ. Sci. Technol.*, 2009, **43**, 2482–2488.

21 Y. Yoshinaga, T. Akita, I. Mikami and T. Okuhara, *J. Catal.*, 2002, **207**, 37–45.

22 O. S. G. P. Soares, J. J. M. Órfão, J. Ruiz-martínez, J. Silvestre-albero and A. Sepúlveda-escribano, *Chem. Eng. J.*, 2010, **165**, 78–88.

23 S. Hamid, S. Golagana, S. Han, G. Lee, M. Babaa and W. Lee, *Chemosphere*, 2020, **241**, 125115.